Journal of Alloys and Compounds 509 (2011) 4065–4072

Contents lists available at ScienceDirect

Journal of Alloys and Compounds

journal homepage: www.elsevier.com/locate/jallcom

Investigation on the synthesis and quantum confinement effects of pure and Mn^{2+} added $Zn_{(1-x)}Cd_xS$ nanocrystals

R. Sakthi Sudar Saravanan [a,*], D. Pukazhselvan [b], C.K. Mahadevan [a]

[a] Physics Research Centre, S.T. Hindu College, Nagercoil 629 002, Tamilnadu, India
[b] Hydrogen Energy Centre, Department of Physics Banaras Hindu University, Varanasi, India

ARTICLE INFO

Article history:
Received 23 November 2010
Received in revised form
27 December 2010
Accepted 29 December 2010
Available online 4 January 2011

Keywords:
Semiconductors
Microwave synthesis
Quantum dots
Dielectric
Exciton bohr radius

ABSTRACT

$Zn_{(1-x)}Cd_xS$ and $Zn_{(1-x)}Cd_xS:Mn^{2+}$ semiconductor quantum dots (2–4 nm) have been prepared by a novel solvothermal route assisted microwave heating method. The growth parameters governing the smaller size and higher yield have been optimized. The synthesized QDs exhibit a significant blue shift as compared to their corresponding bulk counterpart in the UV–vis optical absorption spectrum. The dielectric constant value varies from 2.79 to 6.17 (at 40 °C, 1 kHz) depending upon the composition of the alloy; lower value corresponds to $Zn_{0.75}Cd_{0.25}S:Mn^{2+}$ and the higher value corresponds to $Zn_{0.25}Cd_{0.75}S:Mn^{2+}$. The crystallite size to exciton bohr radius ratio being <1 indicates a strong quantum confinement effect in both CdS and ZnS QDs. The quantum confinement effect exists in the sequence of $ZnS:Mn^{2+} < Zn_{(1-x)}Cd_xS:Mn^{2+}$ ($x < 0.5$) < ZnS < $Zn_{(1-x)}Cd_xS$ < CdS < $CdS:Mn^{2+}$.

1. Introduction

Group II–VI semiconductor nanomaterials/quantum dots (QDs) are promising candidates for optoelectronic applications [1]. Recently, it has been shown that the optical characteristics of semiconductors such as CdS and ZnS can be fine tuned by suitable doping and size effects [2]. Material tailoring of CdS/ZnS/Zn_xCd_yS QDs with and without dopants has therefore gained considerable importance in semiconductor technology [3]. For controlling the growth and agglomeration of QDs, methods such as precipitation within inverted micelles [4], capping techniques [5], synthesis in templates or porous materials [6,7], gels [8] and substrates [9] have been attempted. In spite of these extensive efforts, achieving smaller dot size with high quantum confinement effect (crystallite size/exciton bohr radii < 1) remains a challenging task. To the best of our knowledge, so far, there have been only very few results on the ZnS–CdS system where the size of the dots got restricted to less than 5 nm. Given with this background, in the present investigation, we have synthesized QDs of $Zn_{(1-x)}Cd_xS$ and $Zn_{(1-x)}Cd_xS:Mn^{2+}$ ($x = 0$, 0.25, 0.5, 0.75 and 1) semiconductors through a simple solvothermal-microwave heating method and explored their quantum confinement characteristics. For controlling the size of quantum dots many factors such as, ratio of the reactants, choice of the solvents, annealing temperature and the duration of microwave irradiation have been carefully analyzed and optimized. The structural and microstructural features of the as-prepared materials have been verified by XRD and electron microscopic techniques. The UV–vis spectral analysis reveals that there is a significant blue shift in the optical absorption characteristics, which is an indicative of the smaller size of as-synthesized materials. The solvothermal microwave irradiation technique we employed in the present investigation is much cost effective, high yielding and the result are very encouraging for optoelectronic applications.

We have also studied the dielectric and quantum confinement behavior of the as-prepared QDs. It is known that quantum confinement effects arise when the size of the particles fall below the exciton bohr radius of the material [10]. When the crystal (grain) size is smaller than the electron mean free path, grain boundary scattering dominates which results to dramatic changes in electrical conductivity/resistivity and polarizability, etc. [11]. Since the electrical property and charge confinement effect of QDs can be accounted by dielectric constant we have initially monitored the dielectric constant variation of all the synthesized materials. It has been observed that the composition $Zn_{0.75}Cd_{0.25}S:Mn^{2+}$ results to lowest dielectric constant (2.79) and $Zn_{0.25}Cd_{0.75}S:Mn^{2+}$ results to highest value (6.17) of dielectric constant (40 °C, 1 kHz). The crystallite size to exciton bohr radius being less than 1 illustrates strong quantum confinement behavior of the quantum dots discussed in the present study.

* Corresponding author. Tel.: +91 9443483449.
E-mail address: rsakthiss@yahoo.com (R.S.S. Saravanan).

0925-8388/$ – see front matter © 2011 Elsevier B.V. All rights reserved.
doi:10.1016/j.jallcom.2010.12.198

2. Experimental methods

Analytical reagent (AR) grade zinc chloride monohydrate, zinc acetate dihydrate, cadmium chloride, cadmium acetate dihydrate, manganese(II) acetate tetrahydrate, sodium sulphide and thiourea were purchased from Merck Chemicals. Ethylene glycol was purchased from Central Drug House (P) Ltd, India. These compounds were used without further purification for the preparation of $Zn_{(1-x)}Cd_xS$ and $Zn_{(1-x)}Cd_xS$ with 5 wt.% Mn^{2+}, where $x = 0$, 0.25, 0.5, 0.75 and 1. Metal bearing precursors and sulphur bearing precursors are taken in 1:y (y = 1–3) molecular ratio. The fine mixture of the reactants was then dissolved in 100 ml of the chosen solvent (either double distilled water or ethylene glycol) and kept in a domestic microwave oven (operated with frequency 2.45 GHz and power 800 W) until the solvent gets evaporated. The colloidal precipitate obtained was cooled to room temperature naturally and washed several times firstly with doubly distilled water and then with acetone to remove the organic impurities. The sample was then filtered and dried in atmospheric air. The resultant powder material prepared in the present study was compacted into disc shaped pellets of 13 mm diameter and 1.8 ± 0.2 mm thickness by 5 ton hydraulic pressure. The pelletized samples were annealed for two hours at ~150 °C to achieve densification. After this process, both surfaces of the samples were coated with carbon paste to obtain a good conductive surface layer. The capacitance (C) measurements were carried out to an accuracy of ±1% with Agilant 4284A LCR meter in the temperature range of 40–150 °C and in different frequencies such as 1 kHz, 10 kHz, 100 kHz and 1 MHz. The detailed description of the measurements system is given in our previous work [12]. All the measurement temperature discussed in this paper has been controlled to an accuracy of ±0.5 °C.

X-ray powder diffraction patterns were obtained using an automated PANalytical X-ray powder diffractometer with monochromated Cu K_α radiation (λ = 1.5405 AU). The crystallite size calculation has been performed by pseudo Voigt function method. The use of the Voigt [13] function for the analysis of the integral breadths of broadened X-ray diffraction line profiles forms the basis of a rapid and powerful method of crystallite size determination. In this case, the constituent Couchy component can be obtained from the ratio of full width at half maximum intensity (2ω) and integral breadth (β). The apparent crystallite size 'D' can be related to Couchy (β_c) width of the diffraction peak at the Bragg angle θ;

$$D = \frac{\lambda}{\beta_C \cos\theta} \quad (1)$$

The constituent Couchy component can be given as

$$\beta_C = (a_0 + a_1\psi + a_2\psi^2)\beta \quad (2)$$

$$\psi = \frac{2\omega}{\beta} \quad (3)$$

where a_0, a_1 and a_2 are Couchy constants and β is the integral breadth obtained from PXRD peak.

$$\beta = \frac{\text{Area under the peak}}{\text{Height of the peak}} \quad (4)$$

The values of Couchy constants have been taken from the table of Langford [13] a_0 = 2.0207, a_1 = −0.4803, a_2 = −1.7756.

Optical absorption measurements were done at room temperature using a SHIMADZU UV-2400 PC spectrometer with a medium scan speed sampling interval of 0.5 nm in the wavelength range of 200–700 nm. Microstructural analysis has been performed using SEM Zeiss-SUPRA 40 by secondary electron imaging mode. High resolution imaging of the samples has been performed by Technai G30 Transmission Electron Microscope (TEM).

3. Results and discussion

3.1. Optimization studies

The Cd–Zn–S/Mn nanocrystals can be synthesized by many techniques. However, since the electronic characteristics of this system is extremely sensitive to the size of the particles/crystallites [14] it is convincing only when the synthesis approach provide sizes offering strong quantum confinement effect. It should be noted that, the grain boundary scattering is an important factor governing the quantum confinement characteristics of quantum dots [15]. Therefore, we have paid much attention for optimizing the conditions required for synthesize of smaller Cd–Zn–S/Mn nanoparticles. It is observed that the ratio of the chosen reactants play a major role in controlling the size of the end products. The brief summary of the optimization trials indicating the optimum material out of all the employed materials is given in Tables 1a and 1b. For synthesize of zinc (or cadmium) sulphide, it is observed that only zinc (or cadmium) acetate + thiourea with ethylene glycol solvent yields

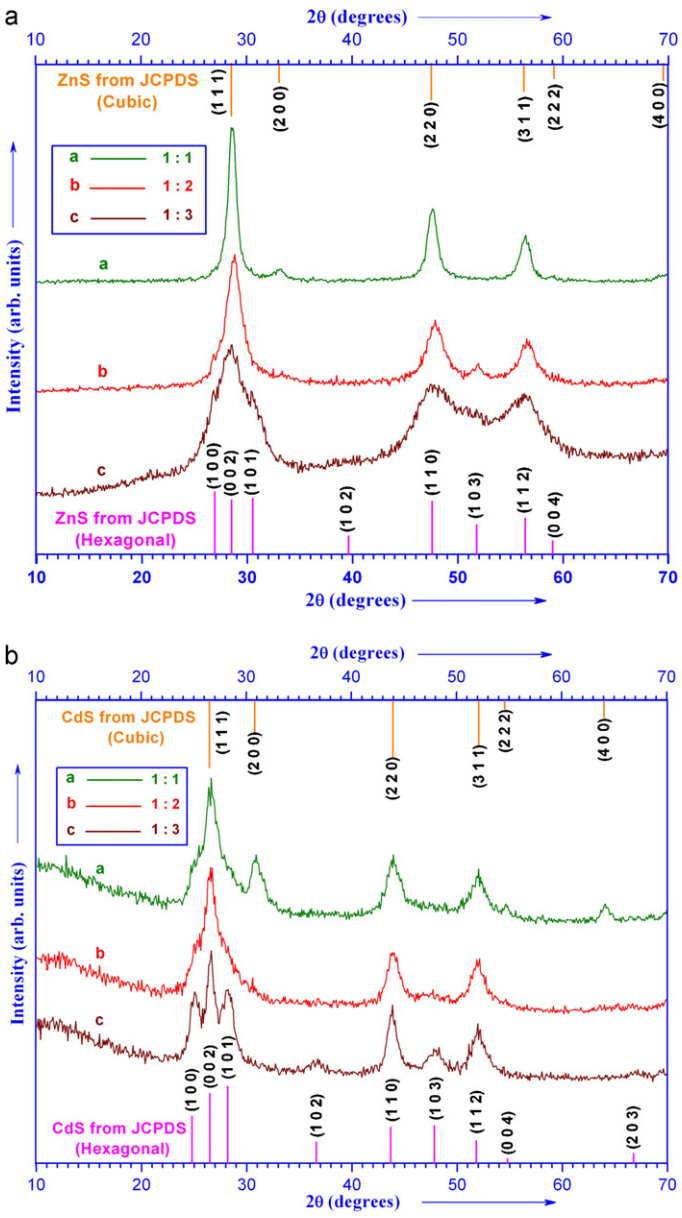

Fig. 1. Powder XRD pattern of (a) ZnS and (b) CdS nanocrystals prepared for zinc acetate/cadmium acetate to thiourea reactant ratios such as 1:1, 1:2 and 1:3 (for details, see text).

fruitful results. Ethylene glycol medium stands superior to distilled water in offering high yield of end product. It is known [16] that the ethylene glycol acting as both reaction media and dispersion media can effectively adsorb and stabilize the surface of the particles. Fig. 1(a) and (b) indicates the XRDs of ZnS and CdS end products for which the reactants were taken in 1:1, 1:2 and 1:3 ratios. As can be clearly seen, XRDs corresponds to higher concentration of thiourea exhibits wide and broadened peaks. This indicates the choice and composition of reactants is a crucial factor to control the size of the end products. While 1:3 ratio seems to be the better composition to achieve smaller crystallite size with higher yield, higher ratios could not be considered in view of the fact that it reduces the effective yield of the product.

3.2. Structural studies

We have also witnessed interesting structural features from both Fig. 1(a) and (b). When the ratio of metal acetate and thiourea

Table 1a
Analysis summary of optimum parameters amongst the different reactants, composition ratios, reaction time, yield percentage and crystallite size of synthesized ZnS nanocrystals.

Reactants	Composition ratio	Solvent	Reaction time (min)	Yield (%)	Size (nm)
Zinc chloride + sodium	1:1	Doubly distilled water	14	14.23	11.5
sulphide	1:2		15	20.58	8.6
	1:3		13	26.59	5.8
Zinc chloride + sodium	1:1	Ethylene glycol	30	18.54	8.8
sulphide	1:2		34	26.81	5.6
	1:3		31	32.93	4.1
Zinc acetate + sodium	1:1	Doubly distilled water	17	23.42	10.3
sulphide	1:2		19	29.64	8.7
	1:3		21	34.73	6.1
Zinc acetate + sodium	1:1	Ethylene glycol	30	29.87	7.6
sulphide	1:2		36	35.64	4.9
	1:3		33	41.12	3.7
Zinc acetate + thiourea	1:1	Ethylene glycol	31	26.71	7.1
	1:2		33	32.94	5.7
	1:3		37	40.04	2.9

is 1:1, the resulting structure is observed to be comparatively bulk with cubic structure. In fact most of the reports in the literature for ZnS/Mn correspond to cubic structure only [17–19]. As we increase the amount of thiourea, there is not only reduction in the crystal size, but also the resulted crystal structure is hexagonal (for both the cases discussed in Fig. 1(a) and (b)). The exact mechanism governing this interesting behavior is not much clear presently. However, since it is known that the packing of atoms per unit volume (packing fraction) in the hcp structure is more perfect than cubic structure, it can be said that the existence of excess sulphur play a key role to a possible dense packing of Cd–Zn–S/Mn structure and fine lattice construction.

Yet another interesting observation is the effect of annealing temperature on the quantum dots. Since we have employed liquid precursors, it is also essential to flush out the volatile impurities by temperature treatment. The solvothermal route yielded products were therefore subjected to annealing at four different temperatures such as 50, 100, 150 and 200 °C. The XRDs of the annealed samples are given in Fig. 2. Careful analysis of these XRD pattern reveals that there are changes in the integral breadth (see Eq. (4)) of the annealed samples which is indicative of crystallite size variation. Fig. 3 shows the effect of annealing temperature on the crystallite size for one of the key compositions namely, $Zn_{0.5}Cd_{0.5}S$. The crystallite size has got decreased from 3.3 nm to 1.8 nm when the annealing temperature was increased from room temperature to 100 °C. However employing further higher temperature results to nanostructures with higher crystallite size. We have observed that annealing at 100 °C provides two interesting results. Firstly, the crystallite size observed at this temperature is the smallest value. Secondly, the samples annealed at temperatures above 100 °C appears to show a directional growth behavior along the (1 1 0) plane. Therefore we considered annealing at 100 °C as another optimum parameter for synthesizing QDs through this method. Detailed X-ray powder diffraction analysis for all the optimized materials was carried out and the results were reported elsewhere [20]. The annealing experiment also provides a clue for tailoring geometrically interesting structures.

High resolution TEM image bringing out the particle size of the as-synthesized material for the composition $Zn_{0.5}Cd_{0.5}S$ is shown in Fig. 4. The diffraction pattern arise from the crystallites is given in the inset. The fine ring pattern reveals the crystallite size is very small. The TEM image also indicates that the derived QDs are self assembled. In the assembly of QDs, few quantum dots with average sizes of ~2 to 4 nm is highlighted by the circular background. It should be mentioned that the self assembling of QDs, commonly referred as self organization of the QDs is a way of self stabilizing the individual dots by forming an assembly. The basic microscopic aspects of assembling, driving the nucleation and evolution of QDs under the role of composition, coverage and intermixing have been given in a comprehensive review of literatures edited by Wang

Table 1b
Analysis summary of optimum parameters amongst the different reactants, composition ratios, reaction time, yield percentage and crystallite size of synthesized CdS nanocrystals.

Reactants	Composition ratio	Solvent	Reaction time (min)	Yield (%)	Size (nm)
Cadmium	1:1	Doubly distilled water	17	29.59	10.4
chloride + sodium	1:2		18	34.11	7.6
sulphide	1:3		16	38.54	5.1
Cadmium	1:1	Ethylene glycol	21	33.85	8.8
chloride + sodium	1:2		18	37.58	5.9
sulphide	1:3		19	42.63	4.6
Cadmium	1:1	Doubly distilled water	23	31.24	11.1
acetate + sodium	1:2		25	36.19	8.4
sulphide	1:3		22	39.98	6.6
Cadmium	1:1	Ethylene glycol	24	30.06	9.3
acetate + sodium	1:2		21	35.67	6.2
sulphide	1:3		25	41.84	4.9
Cadmium	1:1	Ethylene glycol	32	33.57	7.5
chloride + thiourea	1:2		36	38.88	5.9
	1:3		31	43.37	4.7
Cadmium	1:1	Doubly distilled water	19	22.59	12.6
acetate + thiourea	1:2		17	29.86	8.7
	1:3		16	36.24	4.8
Cadmium	1:1	Ethylene glycol	33	28.58	8.6
acetate + thiourea	1:2		34	33.14	5.3
	1:3		36	48.35	3.6

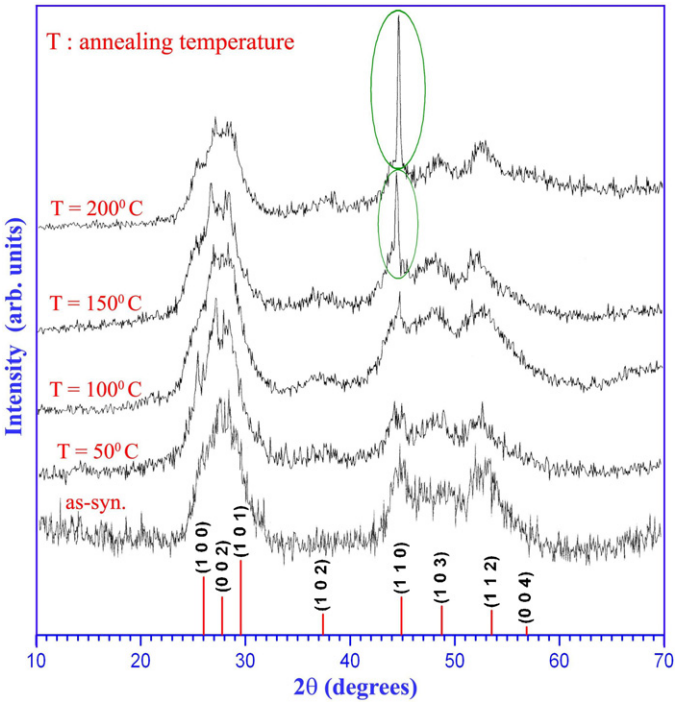

Fig. 2. Powder XRD pattern of $Zn_{0.5}Cd_{0.5}S$ illustrating the effect of annealing temperature. Optimum annealing temperature correspond to100 °C.

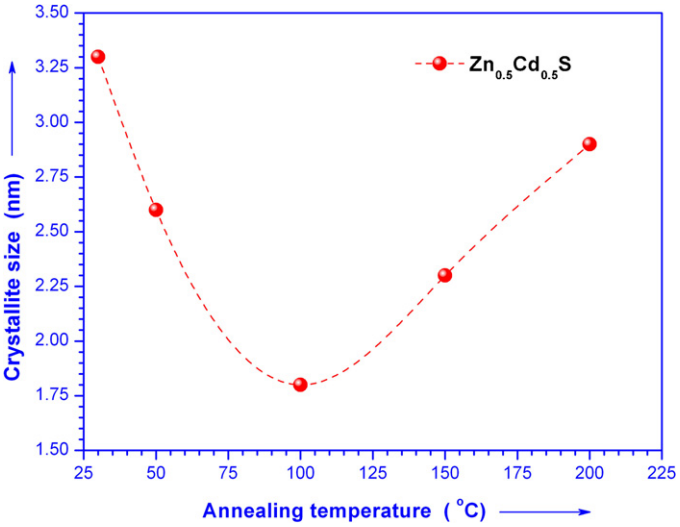

Fig. 3. Relationship between the annealing temperature and the observed crystallite size of $Zn_{0.5}Cd_{0.5}S$.

[21]. We have also observed that the gross microstructure of the as-synthesized product varies by annealing above 100 °C. The SEM microstructural image of the $Zn_{0.5}Cd_{0.5}S$ is shown in Fig. 5. The image of annealed $Zn_{0.5}Cd_{0.5}S$ at 200 °C is given at the inset of Fig. 5. As can be seen, the comparison of microstructure before and after annealing reveals that directional growth indeed occurs as a result of annealing under atmospheric ambient. Therefore it is understood that the sharpening of the peak (1 1 0) upon annealing the sample is a result of the growth of another interesting structure. The directional growth was also found to depend on the choice of ambient. The detailed investigation regarding this will be reported in another communication. The above observation also suggest that, in order to restrict the Zn_xCd_yS material to a dot size (preventing elongation) one should avoid high temperature treatment of the dots.

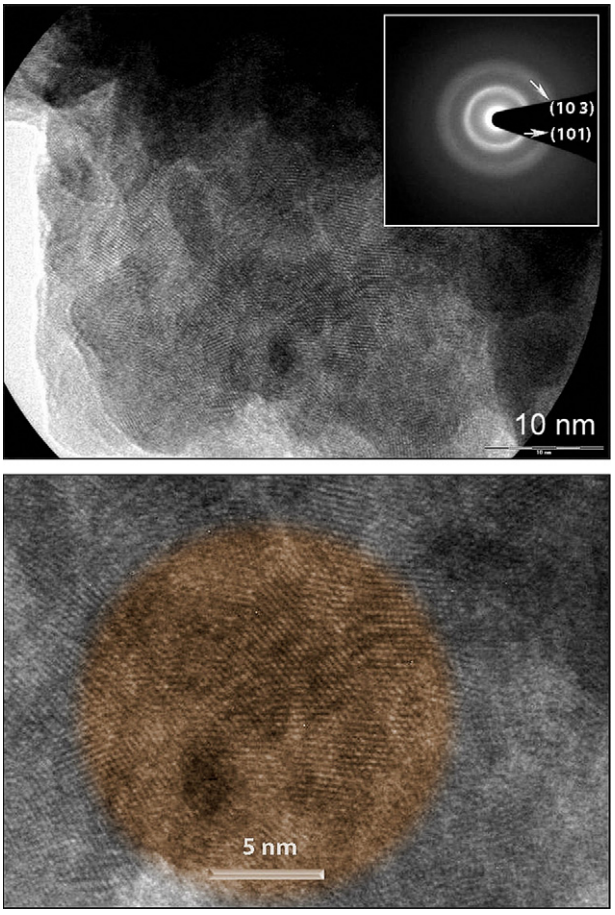

Fig. 4. High resolution TEM image of $Zn_{0.5}Cd_{0.5}S$ quantum dots. (Inset: diffraction pattern obtained from quantum dots, Highlighted background: dispersed fine quantum dots of 2–4 nm diameter.)

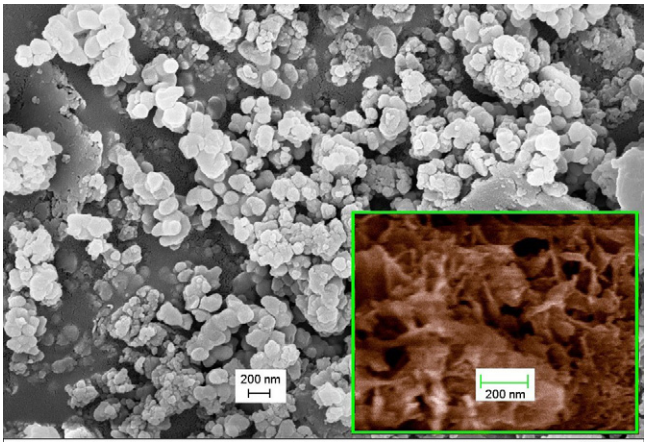

Fig. 5. SEM micrograph depicting the gross microstructure of $Zn_{0.5}Cd_{0.5}S$ nanocrystals/quantum dots. Inset shows the elongated morphology of $Zn_{0.5}Cd_{0.5}S$ as a result of annealing at 200 °C.

3.3. UV–vis absorption studies

Fig. 6(a) and (b) shows the UV–vis optical absorption spectra of all the 10 samples described in the present study. It is clear from the spectrum that both the ZnS, CdS, ZnS:Mn^{2+} and CdS:Mn^{2+} all have got blue shifted in excess of at least 20 nm [22,23] as compared to their bulk counterpart [22–25]. The blue shift occurred in CdS is even more prominent as compared to the bulk CdS system (~90 nm

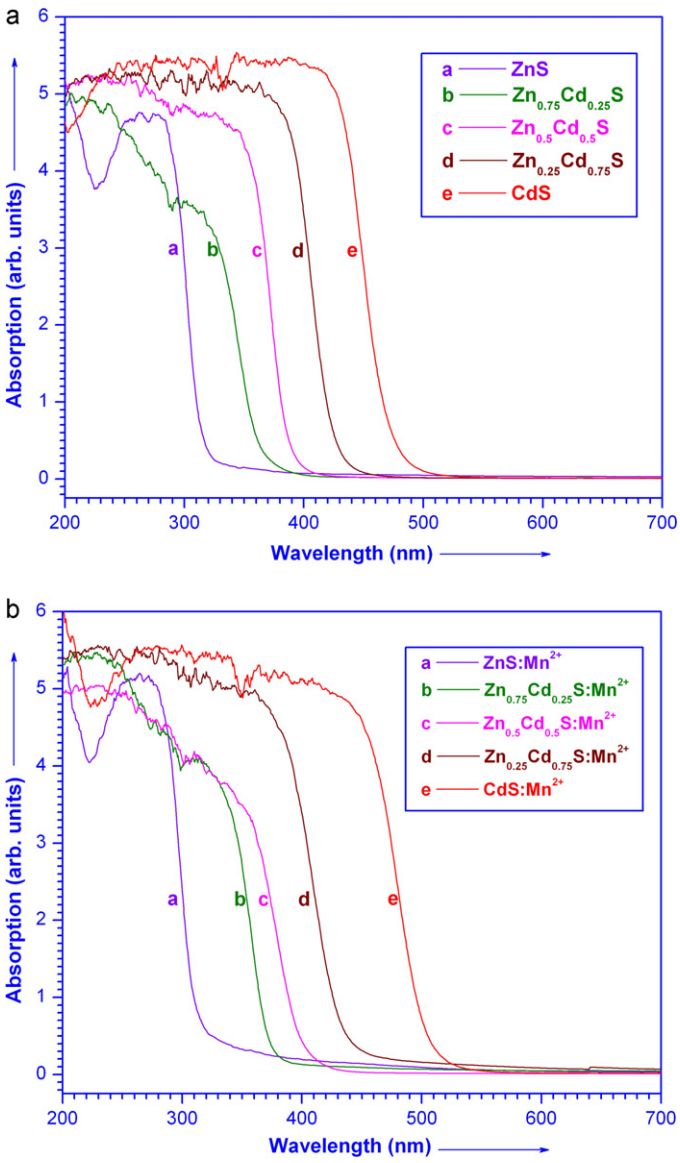

Fig. 6. (a) UV–vis absorption spectrum of pure $Zn_{(1-x)}Cd_xS$ nanocrystals ($x = 0$, 0.25, 0.5, 0.75 and 1). (b) UV–vis absorption spectrum of $Zn_{(1-x)}Cd_xS$ doped with 5 wt.% Mn^{2+} nanocrystals ($x = 0$, 0.25, 0.5, 0.75 and 1).

blue shift) and CdS precipitated in the zeolite matrix (~33 nm blue shift) reported by Sathish et al. [26]. Such effect has been attributed [26] to smaller size induced widening of band gap energy and absorption at lower wavelength. The substitution of Cd in Zn sites results to red shift in all the materials. The obtained optical band gap energy values and the absorption edge have been summarized in Table 2. The peak observed at ~290 nm itself is blue shifted, broad and rather less symmetric. Such nature of excitonic absorption peaks is attributed to the quantum size effect [27]. It is also known that the excitonic peaks get broadened to a wide range when peaks of different exciton energies overlap [28,29]. More importantly, our study indicates that a fine tuning of optical band gap is possible to a desirable range just by changing the size and composition of the material. This is interesting in the context of applications, as for example, Sathish et al. [26] have used the band gap tuned CdS semiconductors for photocatalysis assisted hydrogen production and achieved high hydrogen production rate from water. It should also be noted that the QDs synthesized in the present study is self assembled. However, superior optical characteristics have been observed as compared to the bulk ZnS (3.64 eV)/CdS (2.42 eV)

Table 2
Absorption edge and bandgap values for pure $Zn_{(1-x)}Cd_xS$ and $Zn_{(1-x)}Cd_xS$ doped with 5 wt.% Mn^{2+} nanocrystals ($x = 0$, 0.25, 0.5, 0.75 and 1).

Composition	Absorption edge wavelength (nm)	Bandgap (eV)
ZnS	320	3.878
$Zn_{0.75}Cd_{0.25}S$	373	3.327
$Zn_{0.5}Cd_{0.5}S$	395	3.141
$Zn_{0.25}Cd_{0.75}S$	433	2.863
CdS	492	2.519
$ZnS:Mn^{2+}$	324	3.830
$Zn_{0.75}Cd_{0.25}S:Mn^{2+}$	392	3.161
$Zn_{0.5}Cd_{0.5}S:Mn^{2+}$	408	3.042
$Zn_{0.25}Cd_{0.75}S:Mn^{2+}$	443	2.801
$CdS:Mn^{2+}$	508	2.442

system [30] and other reported ZnS/CdS QD systems [26,31–33]. This also suggests that the self assembling in the present case is a beneficial process and the simple synthesis technique explored in the present study is an interesting alternative for the bulk scale cost effective synthesis of QDs.

3.4. Electrical and quantum confinement studies

In order to understand the effect of composition on the polarizability and charge confinement characteristics of the as-prepared materials we have studied its dielectric characteristics. The profile of dielectric constant with respect to frequency at three different temperatures (40, 100 and 150 °C) for all the concentration is given in Fig. 7(a)–(e). Comparison of the dielectric constant profile of all materials has explored some interesting features. Firstly, the observed dielectric constant is smaller (with frequency 1 kHz) for both ZnS (5.549) and CdS (3.576) as compared to that observed for the bulk crystals (8.76 for ZnS (wurtzite) and 8.64 for CdS (wurtzite) [34,35]). It manifests the important role of size effect in dielectric constant. Secondly, addition of Mn^{2+} on any of the Zn–Cd–S composition makes the polarizability quite temperature sensitive. It can be understood from the high variation of ε_r over different temperature in the Mn^{2+} added composition as compared to Mn^{2+} free composition. Thirdly, the ε_r contribution which arises as a result of Mn^{2+} incorporation gets largely influenced by Cd concentration. One can notice this in 25% Cd ($x = 0.25$) substituted material, where the ε_r value of Mn^{2+} added composition got restricted to lower values as compared to Mn^{2+} free composition (Fig. 7b). On the other hand 75% of Cd ($x = 0.75$) in ZnS has resulted in enhanced ε_r for Mn^{2+} incorporated structures as compared to its Mn^{2+} free counterpart (Fig. 7d). An average variation between these two situations could be observed when Zn and Cd share a 50% ($x = 0.5$) existence in ZnS matrix.

Dielectric constant is attributed to four types of polarizations [36] such as space charge, dipolar, ionic and electronic polarizations. At lower frequencies, since all these four types of polarizations contribute, ε_r value is usually higher. Strong temperature dependent variation of ε_r is attributed to spatial and dipolar polarizations [36,37]. However, the variation of the dielectric constant cannot be solely related to effects of temperature and frequency. In our case the observed smaller value of ε_r for ZnS and CdS QDs as compared to their bulk counterpart suggest the size dependent effects also play a role in ε_r. A recent theory [38,39] which correlates the depolarization effects and free energy has provided some useful insight into the relationship between crystallite size and ε_r. It has been shown that the domain size, boundary thickness and space charge concentration are the main factors affecting the dielectric constant. Any increase in the domain wall thickness reduces the net volume of the individual crystallite and alter the depolarization energy [39]. In addition, it has also been shown that lattice defects, impurities, dislocations and micro strains, etc.

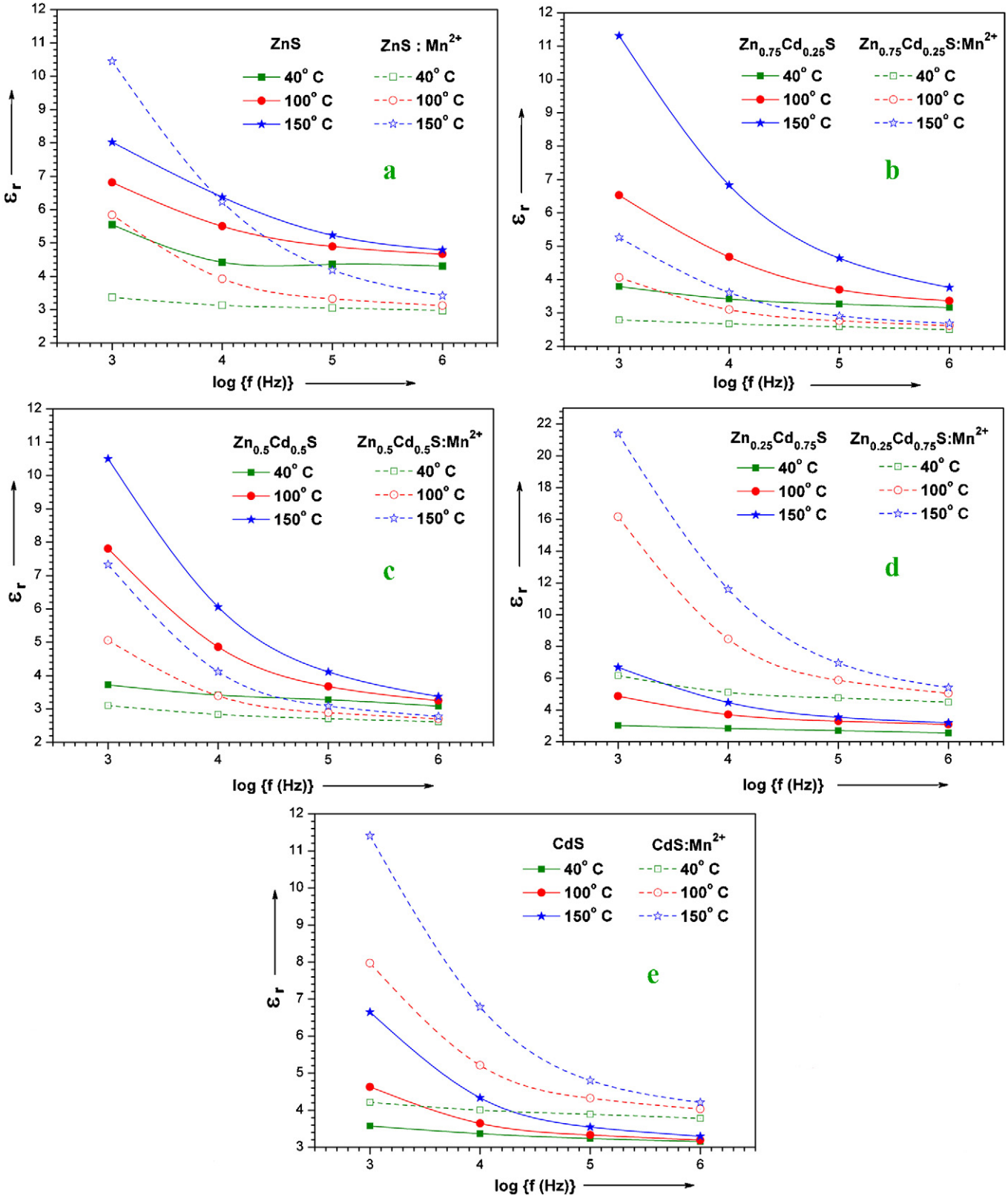

Fig. 7. Variation of dielectric constant with frequency at various temperatures for $Zn_{(1-x)}Cd_xS$ and $Zn_{(1-x)}Cd_xS:Mn^{2+}$ nanocrystals ($x = 0, 0.25, 0.5, 0.75$ and 1): (a) ZnS/ZnS:Mn^{2+}; (b) $Zn_{0.75}Cd_{0.25}S/Zn_{0.75}Cd_{0.25}S:Mn^{2+}$; (c) $Zn_{0.5}Cd_{0.5}S/Zn_{0.5}Cd_{0.5}S:Mn^{2+}$; (d) $Zn_{0.25}Cd_{0.75}S/Zn_{0.25}Cd_{0.75}S:Mn^{2+}$; (e) CdS/CdS:$Mn^{2+}$.

increase dielectric constant. In our case, for all the composition, the crystallite (domain) size is controlled to <1.5 nm with average particle sizes less than 4 nm (for details see our previous communication [20]). From these insights, it is clear that in addition to controlling the size through material tailoring, by substituting Cd and Mn in ZnS matrix one can tune the dielectric properties. Tuning the dielectric property also play a main role in tuning the charge confinement characteristics of semiconductor QDs.

Table 3
Summary of the crystallite size (d_{XRD}) (calculated from Voigt function method), exciton bohr radius (a_B), exciton Rydberg energy (R_y^*) and ratio of crystallite size to exciton Bohr radius (R_{d_{XRD}/a_B}) for $Zn_{(1-x)}Cd_xS$ and $Zn_{(1-x)}Cd_xS$ added with 5 wt.% Mn^{2+} nanocrystals.

Compound	d_{XRD} (nm)	a_B (nm)	R_y^* (meV)	R_{d_{XRD}/a_B}
ZnS	1.41	1.92	75.0	0.73
$Zn_{0.75}Cd_{0.25}S$	1.39	1.97	107.4	0.71
$Zn_{0.5}Cd_{0.5}S$	1.34	2.02	106.7	0.67
$Zn_{0.25}Cd_{0.75}S$	1.32	2.06	128.1	0.64
CdS	1.28	2.11	106.0	0.61
$ZnS:Mn^{2+}$	1.51	1.17	202.8	1.29
$Zn_{0.75}Cd_{0.25}S:Mn^{2+}$	1.4	1.5	191.3	0.93
$Zn_{0.5}Cd_{0.5}S:Mn^{2+}$	1.36	1.83	141.1	0.74
$Zn_{0.25}Cd_{0.75}S:Mn^{2+}$	1.42	2.16	60.1	0.66
$CdS:Mn^{2+}$	1.41	2.49	76.3	0.57

Another interesting observation in our analysis is related with the strong quantum confinement effect of $Zn_{(1-x)}Cd_xS$ and $Zn_{(1-x)}Cd_xS:Mn^{2+}$ ($x=0$ to1). The properties of nanocrystalline materials show deviation from the corresponding bulk properties when the sizes of the crystallites become less or comparable to the exciton bohr radius [40]. The unique electron-hole bound pairing in exciton resembles a hydrogen atom. Therefore, alike to the hydrogen atom, this exciton is characterized by the exciton bohr radius (a_B)

$$a_B = \frac{h^2\varepsilon_r}{4\pi^2 e^2}\left[\frac{1}{m_e^*} + \frac{1}{m_h^*}\right] \quad (5)$$

where ε_r is the dielectric constant, m_e^* and m_h^* are the effective masses of electron and hole respectively, e is the charge and h is the Planck's constant. The effective e–h mass is smaller than the electron mass m_e, and the dielectric constant is usually larger than 1 [41]. Since the polarizability (typified by dielectric constant) varies with respect to the size of the crystallites, it affects the exciton bohr radius also. In the present study, the calculated exciton bohr radii for pure ZnS and CdS are 1.92 and 2.11 nm, respectively and the corresponding exciton Rydberg energies are 75 and 106 meV, respectively. The bohr radius for both the Mn^{2+} free and Mn^{2+} added $Zn_{(1-x)}Cd_xS$ nanocrystals can be calculated from the relation,

$$a_B = 1.92(1-x) + 2.11(x) \quad (x = 0, 0.25, 0.5, 0.75 \text{ and } 1) \quad (6)$$

The results of crystallite size d_{XRD} (calculated from Voigt function method), exciton bohr radius (a_B), exciton Rydberg energy R_y, ratio of crystallite size to exciton bohr radius (R_{d_{XRD}/a_B}) are listed in Table 3. As seen, the crystallite sizes of Mn^{2+} free and Mn^{2+} added $Zn_{(1-x)}Cd_xS$ nanocrystals are less than the corresponding exciton bohr radii (except $ZnS:Mn^{2+}$). The variation of ratio of crystallite size and exciton bohr radius (R_{d_{XRD}/a_B}) for $Zn_{(1-x)}Cd_xS$ and $Zn_{(1-x)}Cd_xS$ ($x=0$, 0.25, 0.50, 0.75 and 1) added with 5 wt.% Mn^{2+} nanocrystals is shown in Fig. 8. It should be noted that the ratio being less than 1 corresponds to strong confinement effect [42]. As seen from the figure, except $ZnS:Mn^{2+}$ all the other compositions lead to strong confinement effect. Substitution of Cd in $ZnS:Mn^{2+}$ strengthen its confinement effect and results in very strong effect when all Zn sites get substituted by Cd. The same substitution trend holds true for Mn^{2+} free compositions as well. Confinement effect in $Zn_{(1-x)}Cd_xS$ is albeit strong, only little variation could be witnessed without Mn^{2+} incorporation. Therefore, it is clear that Mn^{2+} affects the quantum confinement effect of $Zn_{(1-x)}Cd_xS$ and $Zn_{(1-x)}Cd_xS:Mn^{2+}$ to a larger extent. Mn^{2+} addition to Cd rich Zn–Cd–S system leads to high quantum confinement effect and low confinement effect in Zn rich Zn–Cd–S system.

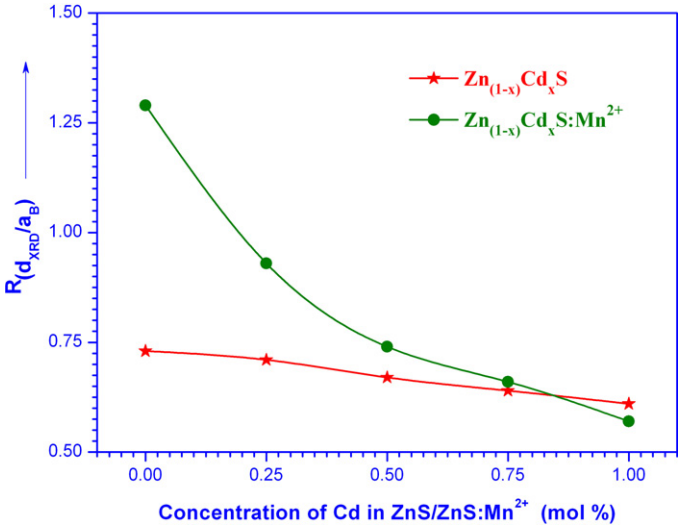

Fig. 8. Crystallite size to exciton bohr radius (R_{d_{XRD}/a_B}) ratio curve depicting the strong quantum confinement effect of $Zn_{(1-x)}Cd_xS$ and $Zn_{(1-x)}Cd_xS$ added with 5 wt.% Mn^{2+} nanocrystals.

4. Conclusions

The optimum material tailoring parameters leading to the formation of $Zn_{(1-x)}Cd_xS$ and $Zn_{(1-x)}Cd_xS:Mn^{2+}$ quantum dots through the present microwave heating method are (i) composition of metal acetate and thiourea in 1:3 ratio, (ii) ethylene glycol solvent medium and (iii) annealing temperature at 100 °C. The novel, cost effective and simple method discussed by us provides quantum size of 2–4 nm which is one of the smallest sizes reported so far. The dielectric constant and charge confinement properties of quantum dots were shown to have fine tuned by choosing the appropriate composition and crystallite size as required for specific applications.

Acknowledgements

One of the authors (C.K. Mahadevan) thanks the council of Scientific and Industrial Research (CSIR) New Delhi for the grant of a Major Research Project.

References

[1] H. Yang, S. Santra, P.H. Holloway, J. Nanosci. Nanotechnol. 5 (2005) 1364–1375.
[2] L. Wang, Y. Jiang, C. Wang, W. Wang, B. Cao, M. Niu, Y. Qian, J. Alloys Compd. 454 (2008) 255–260.
[3] S. Chavhan, R.P. Sharma, J. Phys. Chem. Solids 66 (2005) 1721–1726.
[4] L. Audinet, C. Ricolleau, M. Gandais, T. Gacoin, J.P. Boilot, P.A. Buffat, Philos. Mag. A 79 (1999) 2379–2396.
[5] D. Kim, K.D. Min, J. Lee, J.H. Park, J.H. Chun, Mater. Sci. Eng. B 131 (2006) 13–17.
[6] X. Fu, L. Chen, J. Wang, Y. Lin, H. Shi, Z. Hu, Colloids Surf. A 233 (2004) 189–192.
[7] M.L. Wang, C.H. Wang, W. Wang, Mater. Chem. Phys. 104 (2007) 162–165.
[8] S.M. Reda, Acta Mater. 56 (2008) 259–264.
[9] J. Hiie, T. Dedova, V. Valdna, K. Muska, Thin Solid Films 511–512 (2006) 443–447.
[10] Y. Wang, N. Herron, J. Phys. Chem. 95 (1991) 525–531.
[11] G. Cao, Nanostructures & Nanomaterials: Synthesis, Properties & Applications, Imperial College Press, London, 2004.
[12] C.K. Mahadevan, K. Jeyakumari, Physica B: Condens. Matter 403 (2008) 3990–3996.
[13] Th.H. de Keljser, J.I. Langford, E.J. Mittemeijer, A.B.P. Vogels, J. Appl. Crystallogr. 15 (1982) 308–314.
[14] B. Thomas, M. Abdhulkhadar, Solid State Commun. 94 (1995) 205–210.
[15] L.K. Pan, M.X. Gu, G. Ouyang, C.Q. Sun, Key Eng. Mater. 444 (2010) 17–45.
[16] Y. Ma, E. Vileno, S.L. Suib, P.K. Dutta, Chem. Mater. 9 (1997) 3023–3031.
[17] S. Zu, Z. Wang, B. Liu, X. Fan, G. Qian, J. Alloys Compd. 476 (2009) 689–692.
[18] Y. Shi, J. Chen, P. Shen, J. Alloys Compd. 441 (2007) 337–343.
[19] P. Chawla, S.P. Lochab, N. Singh, J. Alloys Compd. 492 (2010) 662–666.
[20] R.S.S. Saravanan, D. Pukazhselvan, C.K. Mahadevan, Philos. Mag. 91 (2011) 389–403, doi:10.1080/14786435.2010.522214.

[21] Z.M. Wang (Ed.), Self-Assembled Quantum Dots, Lecture Notes in Nanoscale Science and Technology, vol. 1, Springer, 2008, ISBN: 978-0-387-74190.
[22] R. Maity, K.K. Chattopadhyay, Nanotechnology 15 (2004) 812–816.
[23] K.K. Nanda, S.N. Sarangi, S.N. Sahu, Nanostruct. Mater. 10 (1998) 1401–1410.
[24] R.N. Bhargava, D. Gallagher, X. Hong, A. Nurmikko, Phys. Rev. Lett. 72 (1994) 416–419.
[25] H. Yang, P.H. Holloway, Appl. Phys. Lett. 82 (2003) 1965–1967.
[26] M. Sathish, B. Viswanathan, R.P. Viswanath, Int. J. Hydrogen Energy 31 (2006) 891–898.
[27] W.G. Becker, A.J. Bard, J. Phys. Chem. 87 (1983) 4888–4893.
[28] C.N.R. Rao, A. Muller, A.K. Cheetham, The Chemistry of Nanomaterials, vol. 2, Willey-VCH, New York, 2004.
[29] M. Mall, L. Kumar, J. Lumin. 130 (2010) 660–665.
[30] H. Landolt, R. Börnstein, Numerical Data and Functional Relationships in Science and Technology, New Series, Springer-Verlag, Berlin, 1999.
[31] Q. Xiong, G. Chen, J.D. Acord, X. Liu, J.J. Zengel, H.R. Gutierrez, J.M. Redwing, L.C. Lew Yan Voon, B. Lassen, P.C. Eklund, Nano Lett. 4 (2004) 1663–1668.
[32] Y.P.V. Subbaiah, P. Prathap, K.T.R. Reddy, Appl. Surf. Sci. 253 (2006) 2409–2415.
[33] P.K. Ghosh, S. Jana, U.N. Maity, K.K. Chattopadhyay, Physica E 35 (2006) 178–182.
[34] Landolt-Bornstein, Numerical Data and Functional Relationships in Science and Technology, vol. 22A, Springer Verlag, Berlin, 1987, p. 168.
[35] B. Ray, II–IV Compounds, Pergammon Press, New York, 1969.
[36] L.L. Hench, J.K. West, Principles of Electronic Ceramics, John-Wiley and Sons, New York, 1990.
[37] A. Verma, O.P. Thakur, C. Prakash, T.C. Goel, R.G. Mendiratta, Mater. Sci. Eng. B 116 (2005) 1–6.
[38] B.A. Marinkovic, B.D. Stojanovic, V.B. Pavlovic, V.P. Pavlovic, M.M. Ristic, Mater. Struct. 6 (1999) 96–99.
[39] W.Y. Shih, W.H. Shih, I.A. Aksay, Phys. Rev. B: Condens. Matter 50 (1994) 15575–15585.
[40] B. Bhattacharjee, D. Ganguli, K. Iakoubovskii, A. Stesmans, S. Chaudhuri, Bull. Mater. Sci. 25 (2002) 175–180.
[41] S.V. Gaponenko, Optical Properties of Semiconductor Nanocrystals, Cambridge University Press, Cambridge, 1998.
[42] D. Chen, L. Gao, Solid State Commun. 133 (2005) 145–150.